Eur. Phys. J. C 12, 323–330 (2000)
Digital Object Identifier (DOI) 10.1007/s100529900238

THE EUROPEAN PHYSICAL JOURNAL C

Z radiation off stops at a linear collider

G. Bélanger[1], F. Boudjema[1], T. Kon[2], V. Lafage[3]

[1] Laboratoire de Physique Théorique LAPTH[a], Chemin de Bellevue, B.P. 110, 74941 Annecy-le-Vieux, Cédex, France
[2] Seikei University, Musashino, Tokyo 180–8633, Japan
[3] High Energy Accelerator Research Organization, KEK, Tsukuba, Ibaraki 305–801, Japan

Received: 7 July 1999 / Revised version: 19 August 1999 / Published online: 16 November 1999

Abstract. We calculate $e^+e^- \to \tilde{t}_1\tilde{t}_1 Z$ at a linear collider. For large splitting between the two stops, the cross section is sensitive to the value of $m_{\tilde{t}_2}$ when this particle is too heavy to be directly produced. The results are compared to $e^+e^- \to \tilde{t}_1\tilde{t}_1 h$

1 Introduction

In the minimal supersymmetric standard model (MSSM), the third generation of sfermions plays a special role both from a theoretical and a phenomenological point of view. Large mixing in the third generation can induce large splitting between left and right-handed squarks leading in particular to a top squark significantly lighter than other sfermions. With the Higgs, the stop could be the lightest scalar of the MSSM and thus particularly interesting to study at a linear collider where the moderate total energy restricts the number of sparticles that can be directly produced.

A large mixing in the stop sector not only drives the lightest stop mass down but also can induce large couplings between the top squark and the Higgs, affecting in many ways the phenomenology of the Higgs. First, radiative corrections due to top and stop can significantly shift the value of the tree-level mass of the Higgs [1,2]. More importantly, the Higgs signals at LHC–Tevatron could be completely different from what is generally expected in the MSSM with no mixing. The main discovery channel at the LHC, the loop-induced direct production $gg \to h \to \gamma\gamma$, can be severely suppressed [3]. Furthermore, one expects modification of the two-photon width of the Higgs and possibly a large cross section for associated Higgs production $\tilde{t}_1\tilde{t}_1 h$ or $\tilde{t}_2\tilde{t}_1 h$ [4–7], where $\tilde{t}_1(\tilde{t}_2)$ is the lightest (heaviest) top squark.

From the theoretical point of view, there is also ample motivation for considering scenarios of light third-generation sfermions. For example, in inverted hierarchy models, only sfermions of the third generation are light enough to be accessible at LHC/Tevatron or a future linear collider, all others being above the TeV scale [8,9]. Even in models where one assumes universality of sfermion masses at a high scale, the degeneracy is lifted once the masses are run down to the weak scale according to the renormalization group equations, and a light $\tilde{t}_1$ is obtained particularly in models with nonnegligible trilinear couplings. These models are especially attractive, since they solve the supersymmetric flavor problem while preserving the naturality argument. Another motivation for considering a light stop is the possibility of obtaining electroweak baryogenesis [10].

In scenarios with a light stop, as was pointed out in [11–13], the stop pair production at a polarized linear collider can provide a measurement of both the stop mass and the mixing angle. It was also pointed out that provided there is sufficient phase space, the associated production of stops with a Higgs ($e^+e^- \to \tilde{t}_1\tilde{t}_1 h$) could be observable at a high-energy linear collider for some region of the parameter space [7,14]. In fact, in the presence of mixing (associated with a large trilinear term A_t) and a heavy $\tilde{t}_2$, the coupling of the Higgs to $\tilde{t}_1$ becomes very large. In [14] we advocated using the information from $\tilde{t}_1\tilde{t}_1 h$, combined with the measurement of M_h, to extract the value of $\tan\beta$ and $m_{\tilde{t}_2}$; the $\tilde{t}_2$ would be too heavy to be directly produced through $e^+e^- \to \tilde{t}_1\tilde{t}_2$. This is possible, since to a good approximation, we have shown that apart from $\tan\beta$ the $\tilde{t}_1\tilde{t}_1 h$ vertex depends only on the parameters of the stop sector, and so do the dominant corrections to M_h [14]. However, when $\tilde{t}_1\tilde{t}_1 h$ is kinematically accessible, so is $\tilde{t}_1\tilde{t}_1 Z$. The latter process also contains a diagram with Higgs exchange and is therefore sensitive to the value of the $\tilde{t}_1\tilde{t}_1 h$ coupling. The purpose of this paper is to show that although the dependence on the $\tilde{t}_1\tilde{t}_1 h$ coupling is milder than in $\tilde{t}_1\tilde{t}_1 h$ production, the $\tilde{t}_1\tilde{t}_1 Z$ process features in general a larger cross section and can provide complementary information on the parameters of the stop sector.

2 Stop parameters

The stop sector involves three independent parameters that can be taken as the physical masses of the two squarks

[a] URA 14–36 du CNRS, associée à l'Université de Savoie

and the mixing angle. The stop mass eigenstates are defined through the mixing angle $\theta_{\tilde{t}}$, with the lightest stop, $\tilde{t}_1$,

$$\tilde{t}_1 = \cos\theta_{\tilde{t}}\,\tilde{t}_L + \sin\theta_{\tilde{t}}\,\tilde{t}_R. \quad (1)$$

The mixing angle is related to the off-diagonal term of the mass matrix

$$\sin(2\theta_{\tilde{t}}) = \frac{2\,m^2_{\tilde{t}_{LR}}}{m^2_{\tilde{t}_1} - m^2_{\tilde{t}_2}} = \frac{-2m_t(A_t + \mu/\tan\beta)}{m^2_{\tilde{t}_1} - m^2_{\tilde{t}_2}}. \quad (2)$$

with A_t the trilinear parameter of the top and μ the Higgs mixing parameter, in the notation of [14].

When only one stop is kinematically accessible, as would most likely be the case at the linear collider, stop pair production ($\tilde{t}_1\tilde{t}_1$) allows for the determination of one mass, $m_{\tilde{t}_1}$. Since the cross section features a strong dependence on $\cos^2\theta_{\tilde{t}}$, the amount of mixing can also be determined. This is best done by use of polarized beams. A precision at the percent level has been estimated for the high-luminosity 500-GeV collider [15].

In the decoupling limit of large M_A,[1] it has been shown [14] that the $\tilde{t}_1\tilde{t}_1 h$ vertex depends only on the three parameters of the stop sector, together with $\tan\beta$,

$$V_{\tilde{t}_1\tilde{t}_1 h} \simeq \frac{g}{M_W}\Bigg[\sin^2(2\theta_{\tilde{t}})\frac{(m^2_{\tilde{t}_1} - m^2_{\tilde{t}_2})}{4} + m_t^2 + M_Z^2\cos(2\beta)\left(\left(\frac{1}{2} - \frac{2}{3}\sin^2\theta_W\right)\cos^2\theta_{\tilde{t}} + \frac{2}{3}\sin^2\theta_W\sin^2\theta_{\tilde{t}}\right)\Bigg]. \quad (3)$$

Note that in this approximation, there is no μ dependence in the vertex and that the $\tan\beta$ dependence arises from the small D term. For both $\tilde{t}_1\tilde{t}_1 Z$ and $\tilde{t}_1\tilde{t}_1 h$ processes, the value of $\tan\beta$ affects mainly the computation of the Higgs mass.

The vertex almost vanishes when the stop/top contributions cancel each other. This occurs at

$$\sin^2(2\theta_{\tilde{t}}) \approx \frac{4m_t^2}{m^2_{\tilde{t}_2} - m^2_{\tilde{t}_1}}. \quad (4)$$

At small values of $\sin 2\theta_{\tilde{t}}$, the $\tilde{t}_1\tilde{t}_1 h$ vertex, up to small D terms, is of the same order as the $t\bar{t}h$ vertex, since it is dominated by the m_t^2 term in (3). For large values of the $\tilde{t}_1\tilde{t}_1 h$ vertex, the cross section for $e^+e^- \to \tilde{t}_1\tilde{t}_1 Z$ gets quite large. This occurs for maximal mixing, $\sin 2\theta_{\tilde{t}} \approx 1$, with a large splitting between the two stop physical masses, $m_{\tilde{t}_2} \gg m_{\tilde{t}_1}$. However, it is precisely for this configuration that one has some strong constraints. These will be discussed in the next section.

3 Constraints from M_h, $\Delta\rho$, and CCB

The most stringent constraint generally arises from $\Delta\rho$, which receives contributions from both sbottoms and stops. When there is a large splitting between the masses of squarks, the contribution to the gauge-boson self-energies becomes sizable and grows with the mass of the heavier squark. The soft-breaking mass $m_{\tilde{Q}_L}$ being common to the two members of the SU(2) doublet, one parameter of the sbottom sector is related to that of the stop sector:

$$m^2_{\tilde{Q}_L} = \cos^2\theta_{\tilde{t}} m^2_{\tilde{t}_1} + \sin^2\theta_{\tilde{t}} m^2_{\tilde{t}_2} - m_t^2 - M_Z^2\cos(2\beta)\left(\frac{1}{2} - \frac{2}{3}s^2_W\right) \quad (5)$$

$$= \cos^2\theta_{\tilde{b}} m^2_{\tilde{b}_1} + \sin^2\theta_{\tilde{b}} m^2_{\tilde{b}_2} - m_b^2 - M_Z^2\cos(2\beta)\left(-\frac{1}{2} + \frac{1}{3}s^2_W\right). \quad (6)$$

If we restrict ourselves to the limit of small mixing in the sbottom sector, $\theta_b = 0$, we are left with three free parameters among the five parameters of the third-generation squark sector. These will be taken as the physical masses of the stops and the mixing angle, $\theta_{\tilde{t}}$. In this limit, $\tilde{b}_1 \approx \tilde{b}_L$ and is the only component entering the radiative corrections to $\Delta\rho$. The $\tilde{b}_2$ is now purely $\tilde{b}_R$ and decouples from the constraints. There are essentially three contributions to $\Delta\rho$, which in the limit of small mixing in the sbottom sector simplifies to

$$\Delta\rho = -\sin^2\theta_{\tilde{t}}\cos^2\theta_{\tilde{t}} f(m_{\tilde{t}_1}, m_{\tilde{t}_2}) + \cos^2\theta_{\tilde{t}} f(m_{\tilde{t}_1}, m_{\tilde{Q}_L}) + \sin^2\theta_{\tilde{t}} f(m_{\tilde{t}_2}, m_{\tilde{Q}_L}), \quad (7)$$

where the functions $f(m_1, m_2)$ include both one- and two-loop corrections and are defined in [16]. They vanish for equal masses.

Imposing the constraint that $\Delta\rho \leq 0.0013$ [17], we found, as is shown in Fig. 1, that for large mixing $\sin 2\theta_{\tilde{t}} \approx 1$, the large values of $m_{\tilde{t}_2}$ are ruled out. These results assume a fixed value of $m_{\tilde{t}_1} = 120$ GeV. For a near-maximal mixing angle, the $\tilde{t}_2$ cannot exceed 542 GeV, while for a mixing $\cos\theta_{\tilde{t}} \approx .4$ one can allow $\tilde{t}_2$ up to 900GeV. When $\cos\theta_{\tilde{t}}$ is small, ($\sin 2\theta_{\tilde{t}} \approx 0$) masses in excess of 1 TeV are allowed, as the contributions from the terms with large mass splittings are damped by the factor $\sin^2\theta_{\tilde{t}}$. When $\cos\theta_{\tilde{t}} \approx 1$, there exist both a lower and upper limit on $m_{\tilde{t}_2}$. The region where $m_{\tilde{t}_2}$ is small corresponds to one where the common SU(2) squark mass is very low[2]; all terms give a significant contribution to $\Delta\rho$. It is only when $m_{\tilde{t}_2}$ increases that $m_{\tilde{Q}_L} \approx m_{\tilde{t}_1}$; because of the near degeneracy in mass, this term does not contribute to $\Delta\rho$. Furthermore, there is a near cancellation between the two contributions involving the $\tilde{t}_2$.

A large $\tilde{t}_1\tilde{t}_1 h$ vertex also means an important contribution to the Higgs mass. We have taken the approximate formulas at one-loop [18], including a running top mass to incorporate the leading two-loop corrections. In fact, the correction to the Higgs mass depends on exactly the same combination of parameters as the one entering the $\tilde{t}_1\tilde{t}_1 h$

[1] See [14] for further discussion on the validity of this approximation

[2] Note that when $\cos\theta_{\tilde{t}} \approx 1$, the sbottom mass drops below the direct experimental lower bound

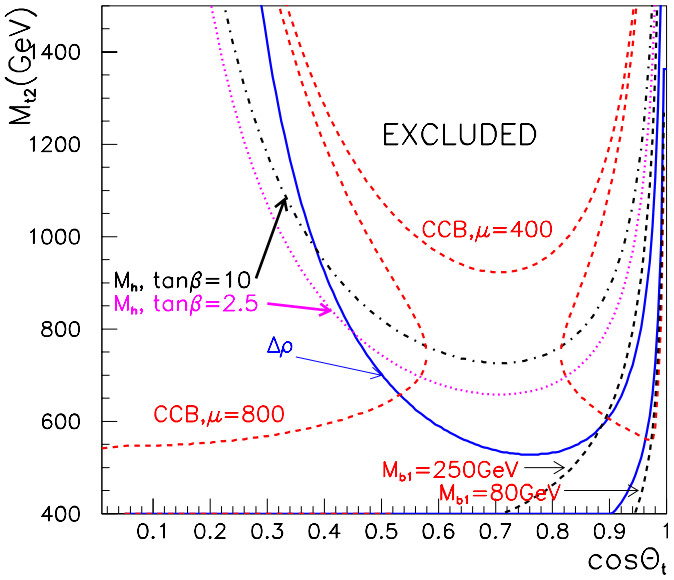

Fig. 1. Constraint from $\Delta\rho \leq 0.0013$ (full line), $M_h \geq 90$ GeV (dash–dotted line), charge-breaking global minima (CCB) (dashed line) and $m_{\tilde{b}_1}$ for $\tan\beta = 10$, $\mu = 400$ GeV, $m_{\tilde{t}_1} = 120$ GeV and $M_A = 1$ TeV. The M_h constraint for $\tan\beta = 2.5$ is also shown (dotted line). The excluded region determined by the above constraints is within the respective boundaries indicated. Note that for $\cos\theta_{\tilde{t}} \approx 1$, the $\Delta\rho$ constraint also excludes the region to the right of the second branch of the $\Delta\rho$ curve where the present limit on the mass of the sbottom is contained. Requiring sbottom production to be above threshold at a 500-GeV linear collider ($m_{\tilde{b}_1} \geq 250$ GeV) excludes the region to the right of the curve. The CCB constraint for $\mu = 800$ GeV is also displayed; the excluded region lies between the two CCB, $\mu = 800$, curves

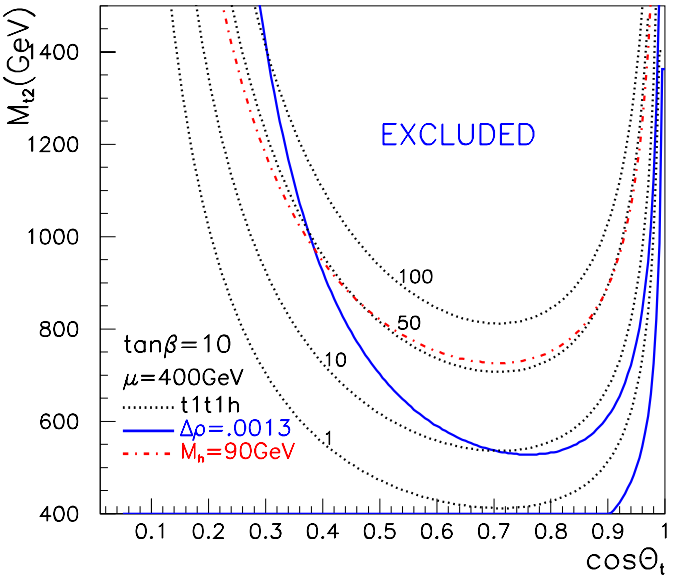

Fig. 2. Equipotential lines (dotted) for the normalized coupling $R_{\tilde{t}_1} = 1, 10, 50, 100$ (see text) with $\tan\beta = 10$ and $\mu = 400$ GeV. The exclusion regions corresponding to $\Delta\rho \leq .0013$ and $M_h \leq 90$ GeV are reproduced from Fig. 1

vertex [14]. For large mixings and large $\tilde{t}_2$ mass, the Higgs mass is driven below the present direct experimental limit, $M_h \leq 90$ GeV and is rapidly driven negative as the $\tilde{t}_2$ mass increases. While the value of the Higgs mass is dependent on $\tan\beta$, there is only a small shift in the allowed region as M_h drops very rapidly when the mixing increases. For the region of large $\sin 2\theta_{\tilde{t}}$, the constraint from $\Delta\rho$ is always more stringent; it is only for mixings below $\approx .4$ that the Higgs mass becomes the most stringent constraint.

One should also note that the constraint arising from the requirement that the parameters do not induce color and charge-breaking global minima (CCB) [19]. An upper bound on A_t or on the amount of mixing follows from this requirement. However, it has been argued that the constraints based on the global minima may be too restrictive [20]. It was shown that for a wide range of parameters, the global CCB minimum becomes irrelevant on the grounds that the time required to reach the lowest energy state exceeds the present age of the universe. Taking the tunneling rate into account results in a milder constraint which may be approximated [20] by:

$$A_t^2 + 3\mu^2 < 7.5\left(m_{\tilde{Q}_L}^2 + m_{\tilde{t}_R}^2\right). \qquad (8)$$

This constraint depends on μ both explicitly and in the calculation of A_t in terms of physical parameters (see (2)). For the parameters we are entertaining here, with an intermediate value for μ, the mild CCB constraint does not come into effect; it is always superseded by both the $\Delta\rho$ and M_h constraints. This value of μ was chosen such that there would not be other supersymmetric particles such as gauginos directly produced at the LC. However, for large values of $|\mu|$ this constraint can become very relevant as both an upper limit and a lower limit on $m_{\tilde{t}_2}$ are obtained. In fact for $\mu = 800$ GeV, the whole area of near maximal mixing is ruled out for any values of $m_{\tilde{t}_2}$. Note that in the region near $\cos\theta_{\tilde{t}} = 1$, the lower bound on $m_{\tilde{t}_2}$ increases significantly; in this region one obtains negative $m_{\tilde{Q}_L}^2$, inducing CCB. The curves for both $\mu = 400$ GeV and 800 GeV are displayed in Fig. 1.

Although the sbottom mass does not enter the calculation of the $\tilde{t}_1\tilde{t}_1 Z$, one has to make sure that the sbottom mass does not drop below the experimental direct bound of roughly 80GeV. This can occur in the region where $\cos\theta_{\tilde{t}} \approx 1$, especially for the low values of $m_{\tilde{t}_2}$. However this constraint is also superseded by the $\Delta\rho$ constraint, Fig. 1. Although it is not strictly a constraint, we are also interested in knowing whether or not the sbottom is light enough to be directly pair-produced at the linear collider. If such is the case, the direct measurement of its mass, at least in the approximation of small mixing, would be sufficient to completely define the parameters of the stop sector. Note that the region where $\tilde{b}_1$ is light enough to be pair-produced corresponds to either small $m_{\tilde{t}_2}$ or $\cos\theta_{\tilde{t}} \approx 1$. In either case, the $\tilde{t}_1\tilde{t}_1 h$ vertex is not large, as can be seen in Fig. 2.

As we are interested in probing the large Yukawa coupling, it is useful to estimate the strength of the $\tilde{t}_1\tilde{t}_1 h$

coupling before going to the full calculation. To this end, we define the coupling squared normalized to the coupling in the no-mixing limit and without a D term; this corresponds approximately to the strength of the $t\bar{t}h$ coupling,

$$R_{\tilde{t}_1} = \left(\frac{M_W V_{\tilde{t}_1 \tilde{t}_1 h}}{g m_t^2} \right)^2 . \quad (9)$$

In Fig. 2, we show contour plots for this normalized coupling for $\mu = 400$ GeV and $\tan\beta = 10$. These curves are based on the exact expression for the vertex (for example, see [14]), including the one-loop corrections to the mass and the coupling of the Higgs. For clarity, the M_h and $\Delta\rho$ constraint discussed above are reproduced there as well. In Fig. 2, one sees that $R_{\tilde{t}_1}$ cannot exceed 50. In fact, the equipotential $R_{\tilde{t}_1} = 50$ almost coincides with the $M_h \geq 90$ GeV exclusion curve, thus it is the maximum enhancement of coupling one can hope for. For certain values of the mixing angle, $\Delta\rho$ excludes lower values of $R_{\tilde{t}_1}$. For example, near the maximal mixing, the $\Delta\rho$ constraint precludes $R_{\tilde{t}_1} \geq 10$, while in the large $\cos\theta_{\tilde{t}}$ region, $R_{\tilde{t}_1}$ could barely exceed 1.

When presenting our results, we will unless otherwise stated impose the limits $M_h > 90$ GeV, $\Delta\rho < .0013$ [21, 17] together with the mild CCB constraint for $\mu = 400$ GeV (8). We also impose a limit on the squark mass, $m_{\tilde{b}_1} \geq 80$ GeV [22].

4 Results

The calculation was performed with the use of the GRACE-SUSY package for automatic calculation of SUSY processes [23]. We modified the tree-level package to include the important radiative corrections to the Higgs mass and couplings. We have included only one-loop corrections for the third-generation squarks. For not-too-large values of $\tan\beta$, the stop contribution completely overwhelms the sbottom contribution. As mentioned above, the relevant parameters are the masses of the stop squarks and the stop mixing angle. The mass of the pseudoscalar is taken to be $M_A = 1$ TeV, while we have chosen $\mu = 400$ GeV. The latter parameter in principle enters the $\tilde{t}_1\tilde{t}_1 h$ vertex but in effect does not influence much the numerical results. Although the $\tilde{b}_2$ does not contribute to the $\tilde{t}_1\tilde{t}_1 Z$ process, we fixed $m_{\tilde{b}_2} = 800$ GeV to ensure that this particle cannot be directly produced even at $\sqrt{s} = 800$ GeV. Because of the reduced phase space available at a 500-GeV collider, we have considered only the case $m_{\tilde{t}_1} = 120$ GeV. For this mass, the cross section for $e^+e^- \to \tilde{t}_1\tilde{t}_1 Z$ can vary by more than an order of magnitude from $\approx .05$–1.5 fb depending on the value of the input parameters as well as on the choice of polarization. Note that this is far from the orders of magnitude variations that we encountered for $\tilde{t}_1\tilde{t}_1 h$ production [14]. Fig. 3 shows how drastically $\tilde{t}_1\tilde{t}_1 h$ changes as $m_{\tilde{t}_2}$ is varied compared to the mild variation of $\tilde{t}_1\tilde{t}_1 Z$. The main reason for this difference is that $\tilde{t}_1\tilde{t}_1 h$ is completely dominated by the $\tilde{t}_1\tilde{t}_1 h$ vertex, whereas in $\tilde{t}_1\tilde{t}_1 Z$ different classes of diagrams contribute (Fig. 4). To get a better understanding of the dependence on the input parameters, it is instructive to consider the contribution from each set of diagrams. The crucial point to note is that some diagrams will involve only gauge couplings, while others will involve Yukawa couplings. The latter are potentially large in the large mass splitting case.

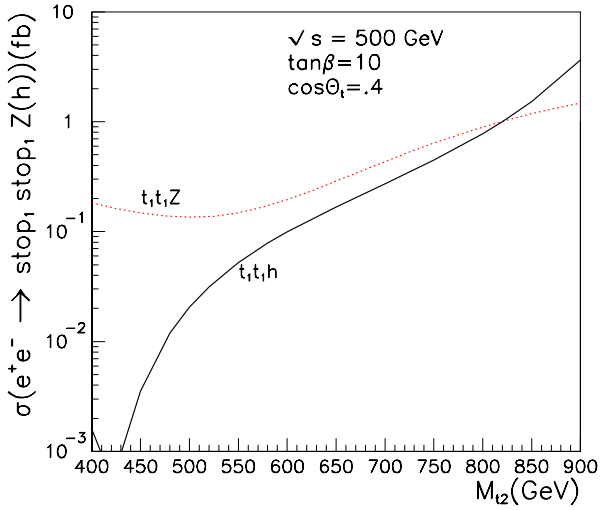

Fig. 3. Comparison of $e^+e^- \to \tilde{t}_1\tilde{t}_1 h$ and $e^+e^- \to \tilde{t}_1\tilde{t}_1 Z$. 100% right-handed e^- polarization is assumed, and $m_{\tilde{t}_1} \approx 120$ GeV

There are four classes of diagrams that enter this process, Fig. 4,

(a) Initial-state Z radiation.
(b) Final-state Z radiation, this includes a diagram with a quartic vertex.
(c) Final-state Z radiation with exchange of a $\tilde{t}_2$.
(d) Higgs exchange diagrams. These also include a diagram involving the exchange of the heavy Higgs; however, this is negligible.

The only diagrams involving the potentially large Yukawa coupling are, besides the Higgs exchange diagram, the ones corresponding to Z radiation off $\tilde{t}_2$ (Fig. 4c). The large Yukawa coupling arises from the Goldstone component of the coupling; thus, when the splitting is large, $\tilde{t}_2 \to \tilde{t}_1 Z$ can be approximated by $\tilde{t}_2 \to \tilde{t}_1\phi^0$, ϕ^0 being the neutral Goldstone boson, with an effective coupling $(g/4M_W)\sin 2\theta_{\tilde{t}}\ (m^2_{\tilde{t}_2} - m^2_{\tilde{t}_1}) = (g/2M_W)m_t(A_t + \mu/\tan\beta)$. Nonetheless, these diagrams also have a $1/(m^2_{\tilde{t}_2})$ factor from the propagator, and we found the overall contribution to the cross section to be rather small. Only the diagram with Higgs exchange will then feature a Yukawa coupling enhancement, and hence a $m_{\tilde{t}_2}$ dependence through the $\tilde{t}_1\tilde{t}_1 h$ coupling. This diagram will contribute to the cross section according to the strength of the $\tilde{t}_1\tilde{t}_1 h$ vertex, from negligible to almost 100%, as Fig. 5 shows. In fact, the contribution of this diagram can almost be inferred from the cross section $e^+e^- \to \tilde{t}_1\tilde{t}_1 h$, see Fig. 3. As for the Z-radiation diagrams, they are dominated by the contribution from Z radiation off initial beams (an order of magnitude larger than the Z radiation off stops). They account for $\sigma = .2$ fb at $\cos\theta_{\tilde{t}} = 0.4$. For a collider

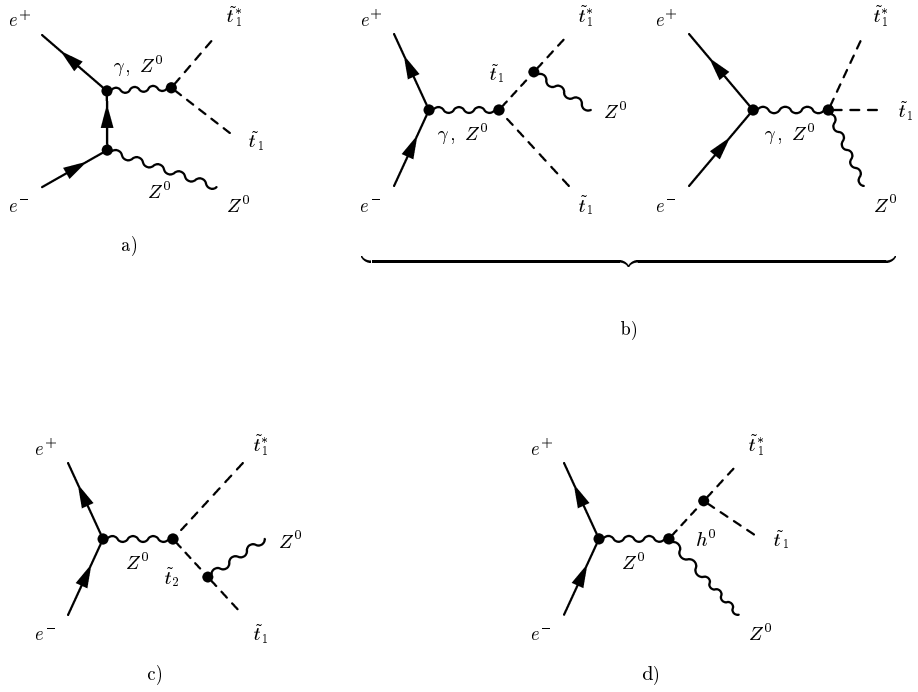

Fig. 4a–d. Classes of Feynman diagrams for $e^+e^- \to \tilde{t}_1\tilde{t}_1 Z$: **a** initial-state radiation; **b** final-state radiation; **c** final-state radiation from $\tilde{t}_2$; **d** Higgs exchange

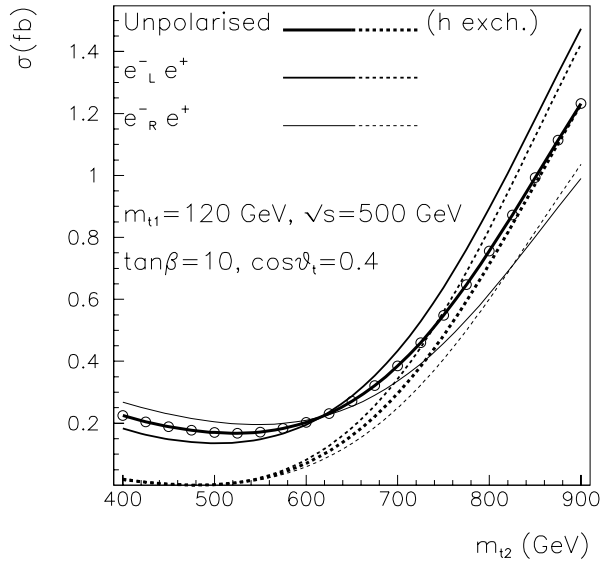

Fig. 5. Polarized and unpolarized cross section for $e^+e^- \to \tilde{t}_1\tilde{t}_1 Z$, $\cos\theta_{\tilde{t}} = 0.4$, $\tan\beta = 10$ and $\mu = 400$ GeV. The contribution of the Higgs exchange diagram is displayed (dashed line)

of luminosity $\mathcal{L} = 500$ fb^{-1}, this corresponds to over 100 raw events. While these events could be recorded and the cross section measured, this would not provide any additional information on the value of the unknown parameter of the stop sector, this could be considered as background events.

To analyze the $m_{\tilde{t}_2}$ dependence of the cross section, first consider the case of intermediate mixing, for example $\cos\theta_{\tilde{t}} = .4$. As was the case for $e^+e^- \to \tilde{t}_1\tilde{t}_1 h$, the cross section is smallest for $m_{\tilde{t}_2} \approx 400$–$600$ GeV, this corresponds to the region where the $\tilde{t}_1\tilde{t}_1 h$ vertex drops significantly. As the $\tilde{t}_2$ mass increases, the cross section increases significantly by almost one order of magnitude. As is reflected in Fig. 5, this is essentially due to the rapidly rising contribution from the Higgs exchange diagram, itself driven by the coupling $\tilde{t}_1\tilde{t}_1 h$. At $m_{\tilde{t}_2} = 900$ GeV, the Higgs diagram alone explains the major part of the cross section, although some important interference effect between the Higgs exchange diagram and all other diagrams remains. In particular, there is some small constructive interference between the initial Z bremsstrahlung and the Higgs contribution and a more important (at the 10% level) destructive interference between the final bremsstrahlung and the Higgs exchange diagram. For this particular value of the mixing angle, the various contributions conspire to cancel each other at the highest mass, and one is left with a cross section which seems to arise nearly 100% from the h exchange diagram. This fortuitous cancellation at $\cos\theta_{\tilde{t}} = 0.4$ does not occur when one looks at the polarized cross section or at any other value of the mixing angle. Note that this behavior is in stark contrast with what was obtained for $e^+e^- \to \tilde{t}_1\tilde{t}_1 h$. There, whenever the $\tilde{t}_1\tilde{t}_1 h$ vertex vanishes, the cross section becomes exceedingly small, since the only diagram that does not contain either $\tilde{t}\tilde{t}h$ vertices, the one originating from $e^+e^- \to hZ$ is completely negligible for the whole range of parameters. Indeed, at high energy, a longitudinal Z, which is essentially a Goldstone boson, would be mainly produced, but this Goldstone boson does not couple to $\tilde{t}_1\tilde{t}_1$. On the other hand, in associated Z production, the same hZ-initiated diagram gives a significant contribution to the cross section, as it is now the Higgs accompanying the longitudinal Z that splits into $\tilde{t}_1\tilde{t}_1$ pairs, and this with a potentially large vertex enhancement.

Next consider the effect of polarization. While for $\tilde{t}_1\tilde{t}_1$ pair production, the value of the stop mixing angle determines the polarized cross section, for the $\tilde{t}_1\tilde{t}_1 Z$ process one has to take into account other parameters as well. In the region where the cross section arises mainly from the diagrams with a Z bremsstrahlung, either initial or final, the polarization dependence is expected to be similar to the one for stop pair production, since essentially gauge couplings which do not change the chirality are involved. In the latter process, the cross section is dominated by e^-_R for $\cos\theta_{\tilde{t}} \leq .5$; otherwise, by e^-_L. However, when the Higgs coupling to $\tilde{t}_1\tilde{t}_1$ becomes large, which for intermediate or large mixing corresponds to the large $m_{\tilde{t}_2}$ region, it is the Higgs exchange diagram that is responsible for most of the cross section (Fig. 5). In this case, the dominant polarization configuration is the same as for an s-channel Z production. The ratio of the polarized cross section is given more or less by the ratio of the couplings of the Z to e_L and e_R, respectively. Note that the difference between the two polarized cross sections is not very pronounced for the value of the mixing we have chosen; it is more marked in the case of small mixing, $\sin 2\theta_{\tilde{t}} \approx 0$. Furthermore, for large $\cos\theta_{\tilde{t}}$, one expects e^-_L to dominate whether or not one benefits from the large Yukawa enhancement. The expectations for different values of $\cos\theta_{\tilde{t}}$ will be discussed next.

For $\cos\theta_{\tilde{t}} \approx 0$, $\sin 2\theta_{\tilde{t}} \approx 0$, one expects from the expression of the $\tilde{t}_1\tilde{t}_1 h$ vertex (3) a very mild dependence on the $\tilde{t}_2$ mass (see Fig. 6). Because the m_t^2 contribution cancels against the mixing contribution, as $\cos\theta_{\tilde{t}}$ increases the strength of the $\tilde{t}_1\tilde{t}_1 h$ vertex decreases until, for $\cos\theta_{\tilde{t}} = .2$ and $m_{\tilde{t}_2} = 900$ GeV, there is a precise cancellation between the stop/top term in the vertex. One is then left with only the contribution from the bremsstrahlung diagrams. Only when the mixing becomes significant can one see a rise in the cross section at large masses. As was discussed in the previous section, the $\Delta\rho$ constraint eliminates the upper range of cross section; this is indicated by dots in Fig. 6. In fact, when mixing reaches $\cos\theta_{\tilde{t}} = 0.6$, the maximum value for $m_{\tilde{t}_2} \approx 600$ GeV and $\sigma \leq 0.4$ fb[3]. For large $\cos\theta_{\tilde{t}}$, because of the $\Delta\rho$ constraint (see Fig. 2) one does not benefit from the strong enhancement of the vertex, and σ cannot exceed 0.3 fb. Furthermore, in these configurations, the sbottom is often directly accessible in the pair production process; this is indicated by an arrow in Fig. 6. The numerical results confirm what we had anticipated in the previous section: Whenever the sbottom can be pair-produced, there is not much interest in the three-body processes. This point concerns not only the $\tilde{t}_1\tilde{t}_1 Z$ but also $\tilde{t}_1\tilde{t}_1 h$ production, as this is just a reflection of the strength of the $\tilde{t}_1\tilde{t}_1 h$ vertex.

The polarized cross sections follow approximately the same pattern; see Fig. 7. As expected, the e^-_L is dominant for large $\cos\theta_{\tilde{t}}$; the cross section can reach 0.75 fb even for a low mass $m_{\tilde{t}_2} = 400$ GeV at $\cos\theta_{\tilde{t}} = .9$. The same polarization dominates also for intermediate $\cos\theta_{\tilde{t}}$ provided $m_{\tilde{t}_2}$ is large; that is, large Yukawa coupling. Otherwise, the choice of a right-handed electron polarization gives a larger cross section.

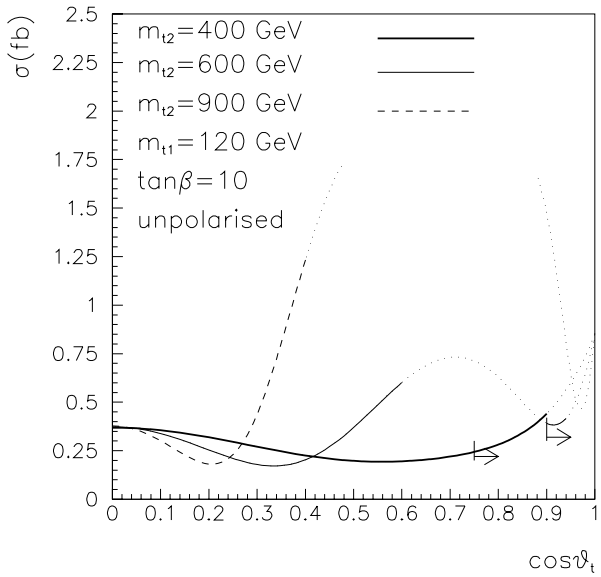

Fig. 6. $\sigma(e^+e^- \to \tilde{t}_1\tilde{t}_1 Z)$ vs $\cos\theta_{\tilde{t}}$ for $m_{\tilde{t}_1} = 120$ GeV $m_{\tilde{t}_2} = 400, 600, 900$ GeV. Points that do not pass the constraints are indicated as dots. To the right of the arrows, $\tilde{b}_1$ pair production opens up ($m_{\tilde{b}_1} \leq 250\ GeV$)

For all numerical results presented we have taken $m_{\tilde{t}_2} \leq 900$ GeV, the maximum value allowed for $\cos\theta_{\tilde{t}} = 0.4$. However one should keep in mind that for smaller values of $\cos\theta_{\tilde{t}}$, the large Yukawa enhancement of the cross section occurs for $\tilde{t}_2$ masses above 1 TeV, which still passes all constraints; see Fig. 1. Nevertheless, for these angles the fluctuations with $m_{\tilde{t}_2}$ are never dramatic and lie within the 3σ interval with a high-luminosity $\mathcal{L} = 500$ fb^{-1}.

We have already alluded to some of the differences between associated Higgs and associated Z production. The main point is that one does not expect as sharp a dependence on the $\tilde{t}_1\tilde{t}_1 h$ vertex (that is, on $m_{\tilde{t}_2}$ for a given mixing angle) as on the process $\tilde{t}_1\tilde{t}_1 h$ itself, since only one diagram contributing to the $\tilde{t}_1\tilde{t}_1 Z$ cross section involves the Higgs. However, as compared to the latter, the associated Z channel features a larger cross section for a large range of parameters. It could therefore be used in conjunction with the associated Higgs channel to help determine the parameters of the stop sector, in particular the mass of the $\tilde{t}_2$ (Fig. 3). For example, assuming an efficiency of 50% and an intermediate value for $\sigma = .38$ fb at $\cos\theta_{\tilde{t}} = .4$ for unpolarized beams one could deduce from a 3σ measurement a mass $m_{\tilde{t}_2} = 700^{+30}_{-50}$ GeV. The uncertainty is of the same order as that expected in $e^+e^- \to \tilde{t}_1\tilde{t}_1 h$ [14]. For this particular mixing angle, roughly the same precision is expected from either electron beam polarization.

If the lightest stop turns out not to be so light, one would need to go to higher center-of-mass energies to observe some events from the associated production of stop and Z. However, higher energies can also mean more phase

[3] In the maximal mixing region, one hits a nonphysical region where the Higgs mass is driven negative and the cross section cannot even be computed, as is the case for example for $0.42 \leq \cos\theta_{\tilde{t}} \leq 0.88$ when $m_{\tilde{t}_2} = 900$ GeV

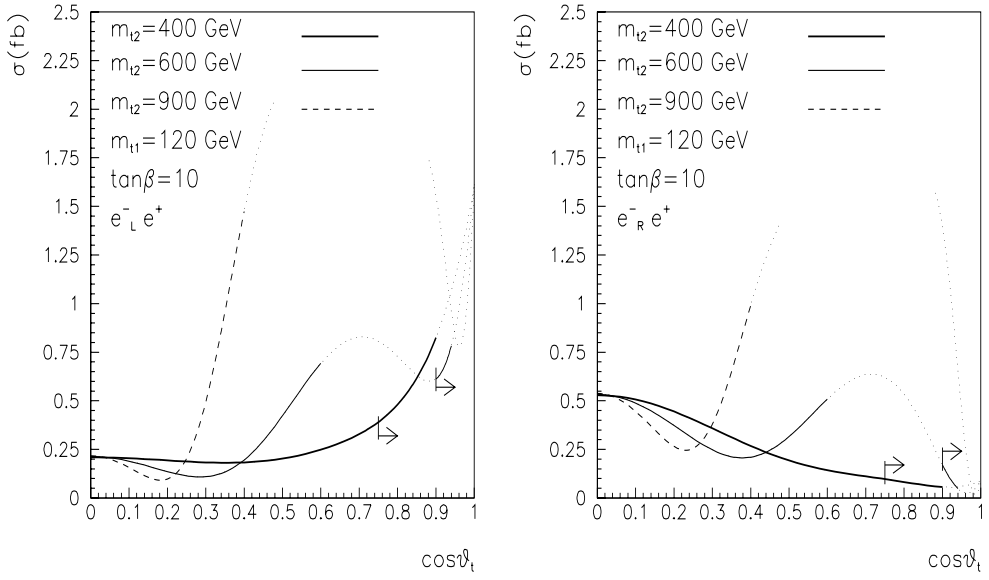

Fig. 7. $\sigma(e^+e^- \to \tilde{t}_1\tilde{t}_1 Z)$ vs $\cos\theta_{\tilde{t}}$ for $m_{\tilde{t}_1} = 120$ GeV, $m_{\tilde{t}_2} = 400, 600, 900$ GeV with polarized beams. The meaning of the dotted lines and the arrows is the same as in the previous figure

space for the direct production process $e^+e^- \to \tilde{t}_1\tilde{t}_2$. Not only could the direct production of $\tilde{t}_2$ allow for the determination of $m_{\tilde{t}_2}$ it can also trigger the final-state $\tilde{t}_1\tilde{t}_1 Z$. This occurs when the $\tilde{t}_2$ further decays in $\tilde{t}_1 Z$. Cross sections of a few fbs can be reached [24], and the partial width into this mode can be quite large, since the $\tilde{t}_2 \to \tilde{t}_1 Z_L$ can benefit from the large Yukawa enhancement, as discussed earlier. This branching fraction depends, however, on the parameters of the MSSM and in particular on those of the sbottom sector. We will not entertain this possibility any longer; here we rather consider only values of the two physical stop masses such that $\tilde{t}_1\tilde{t}_2$ is above threshold. We have considered $\sqrt{s} = 800$ GeV and different values of $m_{\tilde{t}_1}$ while varying $m_{\tilde{t}_2}$ in the range such that $\tilde{t}_1\tilde{t}_2$ is above threshold. In this case we see only a mild dependence on the $\tilde{t}_1\tilde{t}_1 h$ vertex, mostly for the lower values of $m_{\tilde{t}_1}$, Fig. 8. At this energy one can hope for a signal only for $m_{\tilde{t}_1}$ below about 250 GeV.

An important issue that remains to be quantified is the detectability of the signal for both the associated Higgs and the associated Z processes. For the parameters we are considering here, where besides $\tilde{t}_1$, only h and the LSP are light, the only decay mode of $\tilde{t}_1$ is into $c\chi^0$. An analysis of signatures and background for the stop pair production, including the decay mode we are considering, already exists [25]. This issue is also important for the extraction of mass and mixing angle in the pair production. Furthermore, for the precise measurements of these parameters, the question of radiative corrections needs to be taken into account. All the results presented here correspond to a rather large value for μ ($\mu = 400$ GeV); different values of μ could lead to a different MSSM spectrum and eventually different decay modes for the $\tilde{t}_1$. This could even facilitate the extraction of the signal. However, for the production process itself, the numerical results would not differ much in the region that is most interesting, the large mass splitting region, since the contribution from the μ term to the vertex is small compared with the trilinear coupling contribution. Here we have used only one-loop corrections to M_h; the inclusion of the dominant two-loop corrections [2] should not affect the results very much as in associated Z production, we have found very little dependence on the precise value of the Higgs mass.

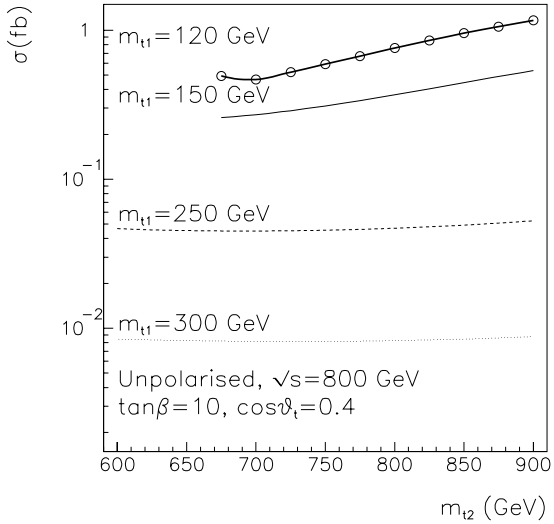

Fig. 8. Cross section for $e^+e^- \to \tilde{t}_1\tilde{t}_1 Z$ at 800 GeV for $m_{\tilde{t}_1} = 120, 150, 250, 300$ GeV, $\cos\theta_{\tilde{t}} = 0.4$, $\tan\beta = 10$, and $\mu = 400$ GeV

In conclusion, the process $e^+e^- \to \tilde{t}_1\tilde{t}_1 Z$ should be measurable at a high-luminosity linear collider such as TESLA, provided the $\tilde{t}_1$ is not very far above the present limit. While observable for any values of the parameters, (our conclusion applies to the small $\tan\beta$ regime), this process can give additional information on the not directly observable $m_{\tilde{t}_2}$, provided there is large mixing and mass splitting. In this sense it is very similar to $\tilde{t}_1\tilde{t}_1 h$. There are regions in parameter space where only the $\tilde{t}_1\tilde{t}_1 Z$ would be observable. In this worst-case situation, even though the cross section does not depend strongly on the parameters,

one can still get a rough determination of a range for $m_{\tilde{t}_2}$. For the intermediate mixing we have discussed at length, nonobservation of $\tilde{t}_1\tilde{t}_1 h$ and a low value for $\tilde{t}_1\tilde{t}_1 Z$ would indicate a $\tilde{t}_2$ in the 400-600 GeV range.

References

1. H. Haber and R. Hempfling, Phys. Rev. Lett.**66**, 1815 (1991); Y. Okada, M. Yamaguchi and T. Yanagida, Prog. Theor. Phys. **85**, 1 (1991); R. Barbieri and M. Frigeni, Phys. Lett. B **258**, 395 (1991); J. Ellis, G. Rigolfi, and F. Zwirner B **262**, 477 (1991)
2. S. Heinemeyer, W. Hollik, and G. Weiglein, Phys. Rev.**D58** (1998) 091701, hep-ph/9803277; *ibid.*, Phys. Lett.**B440** (1998) 296, hep-ph/9807423; *ibid.*, Eur. Phys. J.**C9** (1999) 343, hep-ph/9812472; *ibid.*, Acta Phys. Polon. **B30** (1999) 1985, hep-ph/9903404. The limiting case of vanishing stop mixing and large M_A and $tan\beta$ has been considered by R. Hempfling and A. Hoang, Phys. Lett.**B331** (1994) 99
3. H. Baer, M. Bisset, C. Kao, and X. Tata, Phys. Rev. **D46** (1992) 1067. B. Kileng, Z. Phys. **C63** (1993) 87; B. Kileng, P. Osland, and P.N. Pandita, Z.Phys. **C71** (1996) 87, hep-ph/9506455; G.L Kane, G.D. Kribs, S.P. Martin and J.D. Wells, Phys. Rev.**D50** (1996) 213; A. Djouadi, Phys. Lett. **B435** (1998) 101, hep-ph/9806315
4. G. Bélanger, F. Boudjema, and K. Sridhar, hep-ph/9904348
5. For a study of stop stop Higgs production at the LHC see A. Djouadi, J.L. Kneur, and G. Moultaka, Phys. Rev. Lett.**80** (1998) 1830, hep-ph/9711244
6. A. Dedes and S. Moretti, Phys. Rev.**D60** (1999) 015007, hep-ph/9812328; *ibid.*, RAL-TR-1999-033, hep-ph/9904491
7. A. Djouadi, J.L. Kneur, and G. Moultaka, hep-ph/9903218
8. S. Dimopoulos and G.F. Giudice, Phys. Lett.**357** (1995) 573; A. Pomarol and D. Tommasini, Nucl. Phys.**B466** (1996) 3; G. Dvali and A. Pomarol, Phys. Rev. Lett.**77** (1996) 3728; *ibid.*, Nucl. Phys.**B522** (1998) 3; A.G. Cohen, D.B. Kaplan, and A.E. Nelson, Phys. Lett.**B388** (1996) 588; J.L. Feng, C. Kolda, and N. Polonsky, Nucl. Phys.**B546** (1999) 3, hep-ph/9810500
9. N. Arkani-Hamed and H. Murayama, Phys. Rev.**D56** (1997) 6733; K. Agashe and M. Graesser, Phys. Rev. **D59** (1999) 15007, hep-ph/9801446
10. See for instance J.R Espinosa, Nucl. Phys.**B475** (1996) 273; J.M. Cline, M. Joyce, and K. Kainulainen, Phys. Lett.**B417** (1998) 79, hep-ph/9708393; M. Carena, M. Quirós, and C.E.M. Wagner, Nucl. Phys.**B524** (1998) 3, hep-ph/9710401; J.M. Moreno, M. Quirós, and M. Seco, Nucl. Phys.**B526** (1998) 489, hep-ph/9801272; M. Laine and K. Rummukainen, Phys. Rev. Lett. **80** (1998) 5259, hep-ph/9804255; J.M. Cline, Preprint McGill-98/27, hep-ph/9810267
11. See for instance E. Accomando, et al., Phys. Rep. **299** (1998) 1, hep-ph/9705442
12. A. Bartl, et al., Z. Phys.**C76** (1997) 549, hep-ph/9701336
13. A. Bartl, et al., hep-ph/9709253
14. G. Bélanger, F. Boudjema, T. Kon, and V. Lafage, Eur. Phys. J.**C9** (1999) 511, hep-ph/9811334
15. S. Kraml, talk given at *The ECFA Workshop on Physics at Linear Collider, Oxford, March 1999*; H. Eberl, talk given at the *The ECFA Workshop on Physics at Linear Collider, Sitges, April 1999*
16. A. Djouadi, et al., Phys. Rev. Lett. **78** (1997) 3626; Phys. Rev. **D57** (1998) 4179
17. J. Erler and P. Langacker, hep-ph/9809352
18. J. Ellis, G. Ridolfi, and F. Zwirner, Phys. Lett.**B262** (1991) 477
19. J.M. Frère, D.R.T Jones, and S. Raby, Nucl. Phys.**B222** (1983) 11; M. Claudson, L. Hall, and I. Hinchcliffe, Nucl. Phys.**B228** (1983) 501; C. Kounnas, A.B. Lahanas, D.V. Nanopoulos, and M. Quirós, Nucl. Phys.**B236** (1984) 438; J.F. Gunion, H.E. Haber, and M. Sher, Nucl. Phys.**B306** (1988) 1; P. Langacker and N. Polonsky, Phys. Rev.**D50** (1994) 5824; A. Strumia, Nucl. Phys.**B482** (1996) 24. For a recent summary see J.A. Casas, to be published in *Perspectives on Supersymmetry*, edited by G.L. Kane (World scientific), hep-ph/9707475
20. A. Kusenko, P. Langacker, and G. Segre, Phys. Rev.**D54** (1996) 5824, hep-ph/9602414; A. Kusenko and P. Langacker, Phys. Lett.**B391** (1997) 29, hep-ph/9608340; A. Kusenko, Nucl. Phys. Proc. Suppl. **52A** (1997) 67, hep-ph/9607287
21. The limit on the mass of the SUSY Higgs depends on the SUSY parameters. For an update on the limits on the Higgs mass, see: F. Gianotti, Opal talk for the LEP Committee, March 1999, http://alephwww.cern.ch/ALPUB/seminar/lepc_mar99.pdf. N.J. Kjaer; Delphi talk for the LEP Committee, March 1999, http://delphiwww.cern.ch/delfigs/figures/niels990324.ps.gz; G. Bobbink, L3 talk for the LEP Committee, March 1999, http://l3www.cern.ch/conferences/ps/Bobbink_LEPC9903.ps; and D.A.Glenzinski, Opal talk for the LEP Committee, March 1999, http://www1.cern.ch/Opal/plots/glenzinski/main.ps.gz
22. Aleph Collaboration, Phys. Lett.**B434** (1999) 189, hep-ex/9810028
23. For a description of the program, see for example M. Jimbo, H. Tanaka, T. Kaneko, and T. Kon, hep-ph/9503363; J. Fujimoto, et al., Comp. Phys. Commun. **111** (1998) 185, hep-ph/9711283
24. H. Eberl, S. Kraml, and W. Majerotto, JHEP, **9905** (1999) 016, hep-ph/9903413
25. A. Bartl and W. Majerotto, talk given at the *European Pre-meeting on e^+e^- Collisions at* 500 *GeV, DESY Hamburg, April 2–3, 1993*